A Set-Theoretic Framework to Assess the Impact of Variable Generation on the Power Flow

Xichen Jiang, *Student Member, IEEE*, Yu Christine Chen, *Student Member, IEEE*, and Alejandro D. Domínguez-García, *Member, IEEE*

***Abstract*—The increased penetration of renewable resources, such as wind and solar, into existing power systems introduces significant uncertainties in the generation side. We propose a method to assess whether power system static state variables, i.e., bus voltage magnitudes and angles, remain within acceptable ranges (with some confidence level), as dictated by system operational requirements, while the system is subject to variations in electricity generation arising from the uncertain nature of renewable resources. These variations are assumed to be unknown but constrained to lie (with some confidence level) within some bounded set. Through set operations, we propagate this set through the power flow model, and the result is another set that contains the possible values that (with some confidence level) the state variables (voltage magnitudes and angles) may take. The proposed method is applied to the IEEE 34-bus, and 123-bus benchmark distribution systems.**

I. Introduction

The motivation for this work stems from the push toward environmentally responsible electricity generation, which requires an increased penetration of renewable resources of electricity, such as wind and solar, into existing power systems. Since these resources are intermittent, variable, and difficult to forecast accurately, they introduce additional sources of uncertainty to power systems. This presents notable challenges in system operations across different time-scales—from day-ahead scheduling to automatic generation control. Furthermore, since renewable resources vary in rated power output and point of grid interconnection, they affect power systems at different voltage levels—from transmission to distribution. For example, wind farms are usually connected at the transmission level, whereas small-scale solar installations are usually connected at the distribution level. The focus of this work is on the impact of uncertainty from renewable-based electricity generation connected to distribution systems. In this regard, this paper proposes an analytically tractable method to assess whether system static state variables, i.e., bus voltage magnitudes and angles, remain within acceptable ranges for all possible electric power generation profiles arising from renewable-based electricity sources.

Deterministic power flow analysis, which provides the complex bus voltages given a predetermined generation and load profile at a particular instant in time, is the fundamental tool used by power engineers to determine a snapshot of the power system static states. However, we may be interested in the static states over a range of possible generation profiles to capture the uncertainty associated with renewable-based electricity generation. Previous approaches to assess the effects of uncertainty in the power flow solution can be grouped into probabilistic and set-theoretic methods. In probabilistic power flow analysis (see, e.g., [1]), uncertainties in load and generation are modeled as random variables, which results in the power flow solution also being described by random variables. Both numerical and analytical methods have been proposed to address the probabilistic power flow problem [2], [3], [4], [5]. Also, subsequent research has addressed the issues of efficiency and accuracy in calculating the probability density functions of the bus voltages and line flows [6], [7], [8], [9], [10]. In set-theoretic methods, as applied to study the effect of uncertainty on the power flow solution (see, e.g., [11]), some system parameters and variables are assumed to be unknown, but constrained to lie within a bounded set. For example, in interval analysis [12], [13], [14], [15], it is assumed that some line parameters and loads take values within a symmetric polytope; the resulting power flow solution is then constrained to some symmetric polytope as well. This method has a disadvantage in that this polytope, which contains the set of all possible solutions, may be overly conservative and contains non-solutions.

This paper considers the set-theoretic approach to uncertainty modeling. In our methodology, uncertain variations in renewable-based generation can be viewed as forecast error, which can be bounded (with some confidence level) around the nominal forecast.[1] For example, the power produced by a rooftop solar installation can be assumed to lie within some interval around a nominal power output value, which may be based on forecasted solar insolation level. Then, the set of all renewable-based power generation profiles can be described by a parallelotope (i.e., the generalization of a parallelepiped in three dimensions to higher dimensions). This parallelotope is then bounded by the intersection of a family of ellipsoids, each of which is tight to the parallelotope in a particular direction. Using set operations, each of these ellipsoids is propagated through a model of the power system, which is obtained by linearizing the nonlinear power flow equations. The result is a family of ellipsoids that bound the bus voltage magnitudes and angles. The intersection of this family of ellipsoids approximates the set that describes (with some confidence level) the possible bus voltage magnitude and angle

The authors are with the ECE Department of the University of Illinois at Urbana-Champaign. E-mail: {xjiang4, chen267, aledan}@ILLINOIS.EDU.
Work supported by NSF (USA) under grant ECCS-0925754 and by NSERC (Canada) under its Postgraduate Scholarship Program.

[1]This method is adopted by some system operators to account for uncertainty in wind-based power [16].

realizations. To determine whether renewable-based power generation variability has a significant impact on the power system static performance, we verify that the intersection of this family of ellipsoids is contained within the region of the static state space defined by system operational requirements, e.g., minimum and maximum bus voltage values.

In this paper, we build on our preliminary results reported in [17], extending and improving them in several directions. First, we generalize the input uncertainty set model, which fully accounts for correlation between power injection at different buses as well as asymmetrical uncertainty around a nominal forecast. Additionally, we incorporate a generalized optimization routine, based on the criteria of minimum-trace or minimum-span in an arbitrary direction, to obtain a family of ellipsoids, whose intersection bounds the set of uncertain renewable generation. The optimization routine is general enough to account for correlation between power injections and asymmetrical uncertainty. Furthermore, we expand the performance metric to assess not only the excursions of the voltage magnitudes and angles, but also functions thereof, e.g., active power flows through transmission lines. The scalability of our proposed method to a large number of uncertain power injections is also evinced. We demonstrate these new features in various combinations through several additional case studies. Lastly, we compare the computation time of our method to obtain bounds on the complex bus voltages to that of obtaining nonlinear and linearized power flow solutions.

The remainder of this paper is organized as follows. Section II introduces the fundamental ideas to uncertainty modeling used throughout the paper and illustrates the concepts with a simple example. In Section III, we tailor the ideas presented in Section II to evaluate the impact on system performance of variable generation. Section IV applies the proposed methodology to several benchmark systems, including the IEEE 34-bus and 123-bus test systems. In Section V, we compare the computation time of our method with those of the linearized and nonlinear power flow solutions for the cases presented in Section IV. Concluding remarks are presented in Section VI.

II. Preliminaries: Static Linear System Analysis

In this section, we introduce the basic notions for set-theoretic uncertainty modeling in static linear systems. These techniques are then tailored in Section III to the (nonlinear) power flow problem. To motivate subsequent discussions, consider the linear circuit of Fig. 1. Using Kirchhoff's laws, we obtain the following linear relationship between V_s and i_{load} (referred to as *system inputs*), and the variables v_2 and i_1 (referred to as *system states*):

$$\begin{bmatrix} v_2 \\ i_1 \end{bmatrix} = \begin{bmatrix} \frac{R_2}{R_1+R_2} & -\frac{R_1R_2}{R_1+R_2} \\ \frac{1}{R_1+R_2} & \frac{R_2}{R_1+R_2} \end{bmatrix} \begin{bmatrix} V_s \\ i_{load} \end{bmatrix}. \tag{1}$$

Suppose that the possible values of system inputs V_s and i_{load} are not perfectly known except for some upper and lower bounds. Then, the objective is to characterize the set of all possible values that the system states v_2 and i_1 can take given all possible values that the system inputs can take. We describe next a set-theoretic framework to accomplish this objective.

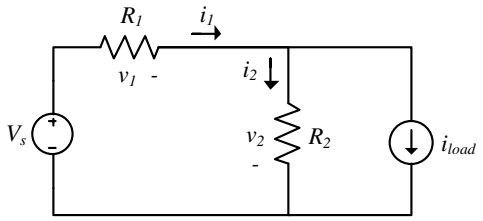

Fig. 1: DC circuit.

A. Unknown-But-Bounded Uncertainty Model

Consider a static linear system described by

$$x = Hw, \tag{2}$$

where $x \in \mathbb{R}^r$ are the system states, $w \in \mathbb{R}^s$ are the system inputs, and $H \in \mathbb{R}^{r\times s}$. Assume that the values w can take are unknown but bounded, i.e., the possible values of w are contained in some closed and bounded set $\mathcal{W} \subseteq \mathbb{R}^s$. Furthermore, we assume that $\mathcal{W}$ is a *parallelotope*, i.e., the generalization of a parallelogram in two dimensions or a parallelepiped in three dimensions to any dimension $s > 3$ (see, e.g., [18]), which can be defined as

$$\mathcal{W} = \{w : w = w_0 + \sum_{j=1}^{s} \alpha_j g_j, \ -1 \le \alpha_j \le 1\}, \tag{3}$$

where $w_0 \in \mathbb{R}^s$ is the parallelotope's center, and $\{g_1, g_2, \ldots, g_s\}$ is a set of independent vectors in $\mathbb{R}^s$. The center w_0 may be interpreted as the nominal operating point of the system in (2) while the set $\mathcal{W}$ captures the uncertainty in w around w_0.

Analogous to the parallelogram, which has two pairs of parallel sides, or a parallelepiped, which has three pairs of parallel faces, a parallelotope has s pairs of parallel *hyper-faces*, with each pair $\{\mathcal{G}_i^+, \mathcal{G}_i^-\}$ defined by

$$\begin{aligned} \mathcal{G}_i^+ &= \{w : w = (w_0 + g_i) + \sum_{j\neq i} \alpha_j g_j, -1 \le \alpha_j \le 1\}, \\ \mathcal{G}_i^- &= \{w : w = (w_0 - g_i) + \sum_{j\neq i} \alpha_j g_j, -1 \le \alpha_j \le 1\}. \end{aligned} \tag{4}$$

1) Significance of the shape of input uncertainty set: It is important to note that the shape of the parallelotope $\mathcal{W}$ captures, to a certain extent, some important features of the uncertain input w. For example, if the vectors $\{g_1, g_2, \ldots, g_s\}$ form an orthogonal basis, then $\mathcal{W}$ is a rectangular parallelotope. In this case, the shape of $\mathcal{W}$ suggests that the value any particular entry of w takes on does not provide additional information on the values that any other entries of w can take, i.e., the entries of w are not correlated. [In a probabilistic setting, the correlation between two random variables can be precisely defined through, e.g., the correlation coefficient. In the context of this work, as our uncertainty model is *not* probabilistic, we use the term correlation in a broad sense to describe an existing relation between mathematical variables which tend to vary or occur together.]

On the other hand, if the vectors $\{g_1, g_2, \ldots, g_s\}$ do not

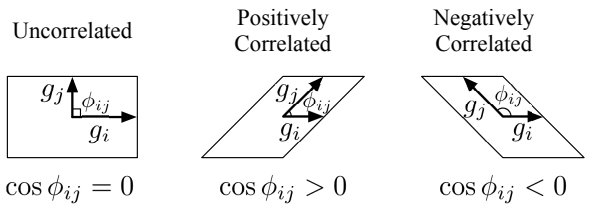

Fig. 2: Significance of input uncertainty set shape.

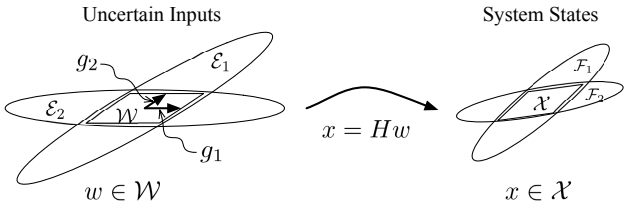

Fig. 3: Ellipsoids $\mathcal{E}_1$ and $\mathcal{E}_2$ bounding $\mathcal{W}$ (the set of all possible values that w can take), and corresponding ellipsoids $\mathcal{F}_1$ and $\mathcal{F}_2$ bounding $\mathcal{X}$ (the set of all possible values that x can take).

form an orthogonal basis, then the angle ϕ_{ij} between each pair of g_i and g_j determines the skewness of $\mathcal{W}$ in certain directions and can be considered as an indicator of how particular entries of w tend to vary together, i.e., they are correlated. [In a probabilistic setting, a similar relationship exists between correlation and orthogonality of random vectors.] In general, larger $|\cos(\phi_{ij})|$ is indicative of higher level of correlation between w_i and w_j, while the sign of $\cos(\phi_{ij})$ indicates whether they are positively or negatively correlated. For the 2-dimensional case, the ideas described above are graphically illustrated in Fig. 2. In the context of this paper, these ideas are important for, e.g., capturing spatial correlation effects between renewable-based power injections.

2) Propagation of input uncertainty set to system states: Given the static linear system in (2) and the input uncertainty set $\mathcal{W}$ defined in (3), the objective is to obtain a set $\mathcal{X} \subseteq \mathbb{R}^r$ (or an upper-bounding approximation) that contains all possible values that x can attain. In order to achieve this, we first approximate the parallelotope $\mathcal{W}$ by the intersection of a family of ellipsoids, $\mathcal{E} = \{\mathcal{E}_1, \mathcal{E}_2, \dots, \mathcal{E}_j, \dots\}$, each of which upper bounds $\mathcal{W}$, i.e.,

$$w \in \mathcal{W} \subseteq \bigcap_i \mathcal{E}_i, \tag{5}$$

with

$$\mathcal{E}_i = \{w : (w - w_0)^T \Psi_i^{-1} (w - w_0) \leq 1\}, \tag{6}$$

where Ψ_i is a positive definite matrix known as the *shape matrix* and w_0 is the center of the ellipsoid $\mathcal{E}_i$. Now, the problem reduces to propagating each ellipsoid $\mathcal{E}_i$ through (2) with the objective of obtaining a set $\mathcal{F}_i$ that contains all possible values of x that result from all possible values that w can take. Since $w \in \mathcal{W} \subseteq \mathcal{E}_i,\ \forall i$, it immediately follows that $x \in \mathcal{X} \subseteq \mathcal{F}_i,\ \forall i$, and hence,

$$x \in \mathcal{X} \subseteq \bigcap_i \mathcal{F}_i. \tag{7}$$

Furthermore, it turns out that ellipsoids are closed under linear transformations; therefore, the set $\mathcal{F}_i$ is also an ellipsoid and can be defined as

$$\mathcal{F}_i = \{x : (x - x_0)^T \Gamma_i^{-1} (x - x_0) \leq 1\}, \tag{8}$$

where $x_0 = Hw_0$ and $\Gamma_i = H\Psi_i H^T$ (see, e.g., [19]). The ideas introduced above are graphically depicted by Fig. 3 for a two-dimensional system with a rhomboidal input set $\mathcal{W}$ — upper bounded by the intersection of two ellipsoids, $\mathcal{E}_1$ and $\mathcal{E}_2$, which map to $\mathcal{F}_1$ and $\mathcal{F}_2$, respectively. As shown in the figure, the intersection of $\mathcal{F}_1$ and $\mathcal{F}_2$ contains the set $\mathcal{X}$. The accuracy of the upper-bounding approximation of $\mathcal{X}$ provided by (7) depends on the choice of the ellipsoids in the family $\mathcal{E} = \{\mathcal{E}_1, \mathcal{E}_2, \dots, \mathcal{E}_j, \dots\}$ upper bounding the set $\mathcal{W}$; we discuss this issue next.

B. Obtaining Input Set Ellipsoidal Bounds

In this section, we provide a method to obtain a family of ellipsoids whose intersection provides a tight over-approximation of the input set $\mathcal{W}$. We also provide an alternative for upper bounding the input set $\mathcal{W}$ with a single ellipsoid $\mathcal{E}_0$; this alternative is computationally more efficient, and, as we show in the case-study section, might suffice in some practical cases.

1) Family of tight upper-bounding ellipsoids: The approach to obtaining a family of ellipsoids $\mathcal{E} = \{\mathcal{E}_1, \mathcal{E}_2, \dots, \mathcal{E}_j, \dots\}$ whose intersection tightly upper bounds $\mathcal{W}$ is to choose each $\mathcal{E}_i$ to contain $\mathcal{W}$ while minimizing its projection onto some direction defined by a unitary vector η_i normal to the hyperplanes $\mathcal{H}_i^+$ and $\mathcal{H}_i^-$ that contain $\mathcal{G}_i^+$ and $\mathcal{G}_i^-$, respectively. The idea behind this choice is as follows. The projection of $\mathcal{E}_i$ onto the direction defined by η_i is in fact the distance between the two most outer points of $\mathcal{E}_i$ that lie in a straight line defined by η_i. Similarly, the distance between $\mathcal{G}_i^+$ and $\mathcal{G}_i^-$ can be obtained by computing the distance between any two points contained in $\mathcal{H}_i^+$ and $\mathcal{H}_i^-$ that also lie in a straight line defined by the vector η_i. Thus, by minimizing the projection of the ellipsoid onto the direction defined by η_i, we obtain an ellipsoid that is tight to the hyper-faces $\mathcal{G}_i^+$ and $\mathcal{G}_i^-$ of $\mathcal{W}$. This is graphically represented in Fig. 4 and formalized in the subsequent discussion.

From (4), it follows that the hyperplanes $\mathcal{H}_i^+$ and $\mathcal{H}_i^-$ that

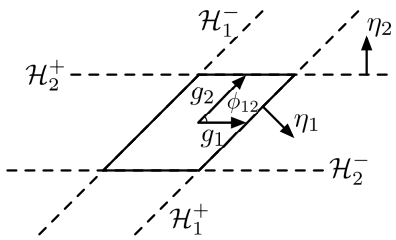

Fig. 4: Hyperplanes ($\mathcal{H}_i^+,\ \mathcal{H}_i^-$) and directions of minimum span (η_i).

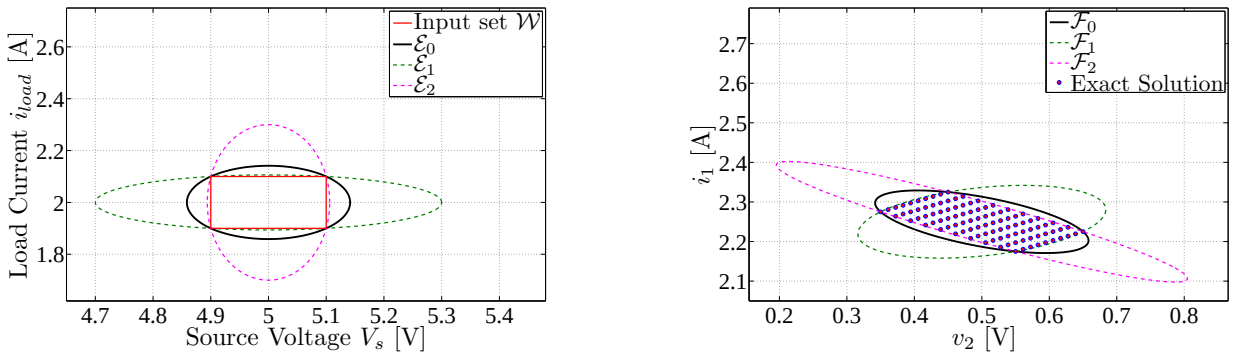

(a) Input uncertainty set and bounding ellipsoids.

(b) State-bounding ellipsoids and exact solution points.

Fig. 5: DC circuit's input and state ellipsoidal bounds.

contain $\mathcal{G}_i^+$ and $\mathcal{G}_i^-$, respectively, are defined by

$$\begin{aligned}\mathcal{H}_i^+ &= \{w : \eta_i^T[w - (w_0 + g_i)] = 0\},\\ \mathcal{H}_i^- &= \{w : \eta_i^T[w - (w_0 - g_i)] = 0\},\end{aligned} \tag{9}$$

where η_i is the normal unitary vector defining the hyperplane $\mathcal{H}_i^+$, i.e., η_i is orthogonal to $\{g_1, g_2, \ldots, g_{i-1}, g_{i+1}, \ldots, g_s\}$ and points outwards with respect to $\mathcal{W}$. Then, η_i is the vector normal to the hyperplane $\mathcal{H}_i^+$ that contains the corresponding hyper-face of the parallelotope as defined in (4). The projection of the ellipsoid $\mathcal{E}_i = \{w : (w - w_0)^T \Psi_i^{-1}(w - w_0) \leq 1\}$ onto the direction defined by η_i is given by $\pi_{\mathcal{E}_i}(\eta_i) = 2\sqrt{\eta_i^T \Psi_i \eta_i}$ [20]. Thus, the problem of obtaining $\mathcal{E}_i$ can be cast into an optimization program as follows:

$$\begin{aligned}\text{minimize} \quad & \sqrt{\eta_i^T \Psi_i \eta_i}\\ \text{subject to} \quad & v^T \Psi_i^{-1} v \leq 1; \qquad \forall v \in \mathcal{V},\\ & \sqrt{\eta_j^T \Psi_i \eta_j} \leq k_j; \quad \forall j \neq i,\end{aligned} \tag{10}$$

where $\mathcal{V}$ is the set of vertices of $\mathcal{W}$, and k_j is the maximum length of the semi-axis in the η_j direction. The first inequality enforces that the resulting $\mathcal{E}_i$ contains $\mathcal{W}$ (the set $\mathcal{V}$ can be obtained from (4) by choosing the α_i's to be 1 and -1). The second set of inequalities constrains the projection of $\mathcal{E}_i$ onto the directions defined by the vectors normal to all other hyperplanes $\mathcal{H}_j^+$, $j \neq i$ and are included for solvability.

Example 1 (DC Circuit): Consider the circuit in Fig. 1, with the relation between inputs, V_s and i_{load}, and states, v_2 and i_1, as given in (1). Let $R_1 = R_2 = 2\ \Omega$; then (1) has the same form as (2) with

$$x = \begin{bmatrix} v_2 \\ i_1 \end{bmatrix}, \ H = \begin{bmatrix} 0.5 & -1.0 \\ 0.25 & 0.5 \end{bmatrix}, \ w = \begin{bmatrix} V_s \\ i_{load} \end{bmatrix}.$$

Suppose that each entry in w is not perfectly known, except that they can vary within certain bounds: $V_s \in [4.9\ 5.1]$ and $i_{load} \in [1.9\ 2.1]$, that is, the source voltage V_s and load current i_{load} are assumed to vary ± 0.1 V and ± 0.1 A around the nominal values of 5 V and 2 A, respectively. Thus, $\mathcal{W}$ is a rectangle, as shown in Fig. 5(a). Now in order to obtain the set $\mathcal{X}$ bounding the system states, we first bound $\mathcal{W}$ with the intersection of two ellipsoids $\mathcal{E}_1$ and $\mathcal{E}_2$ (each of which is tight along an axial direction) as follows: $w \in \mathcal{W} \subseteq (\mathcal{E}_1 \cap \mathcal{E}_2)$; the entries of the corresponding shape matrices Ψ_1 and Ψ_2 are given in Table I. For each input-bounding ellipsoid $\mathcal{E}_i$, $i = 1, 2$, we compute corresponding ellipsoids $\mathcal{F}_i$, $i = 1, 2$, both of which bound $\mathcal{X}$. Additionally, we repeatedly sample the input space $\mathcal{W}$ to calculate the corresponding exact solution of the states using (1). The resulting ellipsoids $\mathcal{F}_i$, $i = 1, 2$, along with the exact solutions (depicted with points), are shown in Fig. 5(b). By inspecting the figure, it is evident that the intersection of the state-bounding ellipsoids provides a tight bound on the exact set to which the states x belong. More precisely, $x \in \mathcal{X} \subseteq (\mathcal{F}_1 \cap \mathcal{F}_2)$, where $\mathcal{F}_1$ and $\mathcal{F}_2$ are the system state-bounding sets that correspond to input sets $\mathcal{E}_1$, and $\mathcal{E}_2$, respectively. The accuracy of the state-bounding set approximation increases as more ellipsoids are used to bound the input space. However, as evidenced in Fig. 5(b), just two ellipsoids $\mathcal{F}_1$ and $\mathcal{F}_2$ establish a reasonably accurate approximation to the exact bounding set for this example. ■

2) Single upper-bounding ellipsoid: While the method described in (10) provides in general an accurate approximation of the input set $\mathcal{W}$ by obtaining a family of ellipsoids $\mathcal{E} = \{\mathcal{E}_i,\ i = 1, \ldots, s\}$, it requires solving the optimization program in (10) for each of input-bounding ellipsoids, up to the dimension of the input set, s; this computation can be parallelized using, e.g., the MATLAB parallel toolbox. In this regard, tightly upper bounding $\mathcal{W}$ results in a very accurate upper-bound on the set $\mathcal{X}$. If the purpose of the analysis is to verify whether or not $\mathcal{X}$ is fully contained in a region Φ of the state space defined by some performance requirements (we further elaborate on this in Section III-C), then it may not be necessary to obtain all the ellipsoids in the family $\mathcal{E}$ but just a subset $\mathcal{E}_q \subseteq \mathcal{E}$. Then, if we compute $q < s$ ellipsoids using (10), and verify that the resulting $\mathcal{F}_i$'s are such that $\cap_{i=1}^q \mathcal{F}_i \subseteq \Phi$, we do not need to compute the remaining $s - q$ $\mathcal{E}_i$'s (and the corresponding $\mathcal{F}_i$'s) as it follows

TABLE I: Entries of shape matrix Ψ_i defining $\mathcal{E}_i$, $i = 0, 1, 2$.

	$\Psi_i(1,\ 1)$	$\Psi_i(1,\ 2) = \Psi_i(2,\ 1)$	$\Psi_i(2,\ 2)$
$\mathcal{E}_0$	0.02	0	0.02
$\mathcal{E}_1$	0.09	0	0.011
$\mathcal{E}_2$	0.011	0	0.09

that $\mathcal{X} \subseteq \cap_{i=1}^{s}\mathcal{E}_i \subseteq \cap_{i=1}^{q}\mathcal{E}_i \subseteq \Phi$. An advantage of this procedure is that, after each new ellipsoid is obtained, we can check whether the intersection of $\mathcal{F}_i$'s satisfies operational constraints and stop when the condition is met.

Following the ideas above, in some cases, it may be convenient to obtain a single bounding ellipsoid for $\mathcal{W}$ and conduct the analysis for just this ellipsoid. While any of the ellipsoids in the family $\mathcal{E} = \{\mathcal{E}_i,\ i = 1, \ldots, s\}$ would serve this purpose, recall that each $\mathcal{E}_i \in \mathcal{E}$ is tight to $\mathcal{W}$ in a particular direction defined by η_l in the sense that projection of of the ellipsoid onto the direction defined by η_l is minimal, but its projection onto other directions $\eta_i,\ i \neq l$ might be much larger than the actual projection of $\mathcal{W}$ onto that direction. Thus, an alternative to this problem is to obtain an ellipsoid $\mathcal{E}_0 = \{w : (w - w_0)^T\Psi_0^{-1}(w - w_0) \leq 1\}$ that minimizes the sum of the projections onto all directions defining the semi-axes of $\mathcal{E}_0$, which is equivalent to minimizing the sum of the squared semi-axes of $\mathcal{E}_0$ [20]. The sum of the squared semi-axis of $\mathcal{E}_0$ is given by the $\tau_{\mathcal{E}_0} = \text{trace}(\Psi_0)$. Thus, the problem of obtaining $\mathcal{E}_0$ can be cast into an optimization program:

$$\begin{array}{ll} \text{minimize} & \text{trace}(\Psi_0) \\ \text{subject to} & v^T\Psi_0^{-1}v \leq 1, \quad \forall v \in \mathcal{V}. \end{array} \tag{11}$$

As we will show in subsequent case studies, the corresponding $\mathcal{F}_0$ that results from (8) is a good first approximation to the exact set that bounds all possible values that the system states can take. Additionally, if $\mathcal{F}_0$ is contained within the state-space region Φ defined by system operational requirements, we can conclude that $\mathcal{X} \subseteq \mathcal{F}_0 \subseteq \Phi$ and no further analysis is needed.

Finally, another alternative to the single ellipsoid $\mathcal{E}_0$ bounding $\mathcal{W}$ that is optimal in some sense is to choose $\mathcal{E}_0 = \{w : (w-w_0)^T\Psi_0^{-1}(w-w_0) \leq 1\}$ such that its volume is minimal. The volume of an ellipsoid is given by $v_{\mathcal{E}_0} = c_n\sqrt{\det(\Psi_0)}$, where c_n is some constant that depends on s (the dimension of the input space). Again the problem of finding $\mathcal{E}_0$ can be cast into an optimization program by replacing the cost function in (11) by $c(\Psi_0) = c_n\sqrt{\det(\Psi_0)}$. In our earlier work in power system uncertainty analysis, we have used this optimality criterion [17].

Example 2 (DC Circuit): Consider again the DC circuit in Fig. 1. We bound $\mathcal{W}$ with a minimum-trace ellipsoid $\mathcal{E}_0 = \{w : (w - w_0)^T\Psi_0^{-1}(w - w_0) \leq 1\}$, where $w_0 = [5\ \text{V}\ 2\ \text{A}]^T$, and Ψ_0 with entries given in Table I; this ellipsoid is plotted in Fig. 5(a) with a solid trace. Now, we can obtain a single ellipsoid $\mathcal{F}_0 = \{x : (x - x_0)^T\Gamma_0^{-1}(x - x_0) \leq 1\}$ that bounds the values of x for all $w \in \mathcal{E}_0$. The shape matrix of this ellipsoid is given by

$$\Gamma_0 = H\Psi_0H^T = \begin{bmatrix} 0.025 & -0.0075 \\ -0.0075 & 0.00625 \end{bmatrix},$$

and the center is given by $x_0 = [0.5\ \ 0.25]^T$. While this minimum-trace ellipsoid does not produce as tight of a bound to the values that the system states can take as the intersection of the minimum-projection ellipsoids in Example 1, it provides a good first approximation to the exact state-bounding set. ■

III. Power System Uncertainty Model

In this section, we tailor the ideas described in Section II to study the impact of uncertainty in renewable-based electricity generation on power system static states, i.e., voltage magnitudes and angles. Renewable-based power generation is described by an unknown-but-bounded uncertainty model. The power flow equations are linearized around a nominal operating point that results from the nominal renewable-based power generation profile. Then, assuming the uncertainty around the nominal power generation profile is small, the linearized model can be used to approximate the set that bounds all possible values that the system states can take.

A. Power Flow Model

As stated in the Introduction, the focus of the paper is on assessing the impact of renewable-based electricity generation connected to distribution systems. As of today, such systems are, in general, mostly radial with a single source of power injection (see, e.g., [21]). However, in order to make the framework general, when formulating the power flow model, we consider the possibility of having a meshed network with multiple sources of power (both conventional and renewable).

Let V_i, and θ_i denote the voltage magnitude and angle of bus i. Additionally, denote by P_i^g and Q_i^g the generation of real and reactive power at bus i. Similarly, denote by P_i^d and Q_i^d the demand of real and reactive power at bus i. Then,

$$\begin{aligned} P &= V_i\sum_{k=1}^{n} V_k\left[G_{ik}\cos(\theta_i - \theta_k) + B_{ik}\sin(\theta_i - \theta_k)\right], \\ Q &= V_i\sum_{k=1}^{n} V_k\left[G_{ik}\sin(\theta_i - \theta_k) - B_{ik}\cos(\theta_i - \theta_k)\right], \end{aligned} \tag{12}$$

where $P = P_i^g - P_i^d$, and $Q = Q_i^g - Q_i^d$; G_{ik} and B_{ik} are the real and imaginary parts of the (i, k) entry in the network admittance matrix, respectively. Assume that bus 1 is the slack bus, and let m denote the number of PQ buses in the system. After removing the active and reactive power equations for the slack bus, and the reactive power equations for the PV buses from (12), we can write the remaining equations as

$$u + w = f(x) + v, \tag{13}$$

where the function $f : \mathbb{R}^{n+m-1} \mapsto \mathbb{R}^{n+m-1}$ takes into account the known bus voltages in the PV buses, and V_1 and θ_1 for the slack bus. In (13), $x \in \mathbb{R}^{n+m-1}$ represents unknown quantities to be solved for, and includes V_i and θ_i for PQ buses and θ_i for PV buses; $u \in \mathbb{R}^{n+m-1}$ contains active power injections in PV buses arising from *conventional* sources, $w \in \mathbb{R}^{n+m-1}$ contains *renewable-based* active power generation in both PV and PQ buses, and reactive power injections in PQ buses; $v \in \mathbb{R}^{n+m-1}$ contains the demand of active power in PV buses, and demand of both active and reactive power injections in PQ buses. Note that in (13), the entries of u corresponding to reactive power balance equations in PQ buses are zero. Similarly, in (13), the entries of w and v corresponding to buses without renewable-based generation and load, respectively, are also zero.

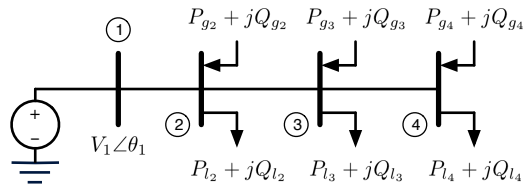

Fig. 6: Four-bus system with renewable power injection.

Since load forecast is, in general, more accurate than renewable-based generation forecast [22], we assume that the uncertainty in load v is negligible compared to that in w; therefore, in (13), uncertainty only enters into w (however, the methodology can be easily extended to include uncertainty in load forecast). Thus, let w_0 denote the nominal value that w takes, resulting from forecast. Then, following the ideas described in Section II, we assume that the values of w are not perfectly known but belong to a parallelotope $\mathcal{W}$ centered around $w = w_0$. Here, it is important to note that the bounds on the variations in w around w_0 are determined by the forecast error; thus, to be precise, $\mathcal{W}$ describes the values that w can take with certain confidence level α, i.e., $\Pr\{w \in \mathcal{W}\} = \alpha$. As already discuss in Section II, the skewness of $\mathcal{W}$ is an indicator of the correlation between renewable-based generation at particular buses. Additionally, the distance between pairs of parallel hyper-faces determines the level of uncertainty in generation.

Example 3 (Four-bus system): In order to illustrate the ideas discussed above, we consider the four-bus system shown in Fig. 6 with renewable-based resources connected to buses 2, 3, and 4. Following the notation in (3), the input set $\mathcal{W}$ that describes the uncertain renewable-based power injection is defined by $w_0 = [P^0_{g2}\ P^0_{g3}\ P^0_{g4}]^T = [0.4\ 0.3\ 0.5]^T$ and $g_1 = [0.08\ 0\ 0]^T$, $g_2 = [0.05\ 0.03\ 0]^T$, $g_3 = [0\ 0.07\ 0.04]^T$, and is shown in Fig. 7(a). From Fig. 7(b), we can conclude that the uncertainty in P_{g3} and P_{g4} are positively correlated. Similarly, Fig. 7(c) shows that the uncertainty in P_{g2} and P_{g3} are also positively correlated. On the other hand, P_{g2} and P_{g4} are uncorrelated, as exemplified by the projection in Fig. 7(d). Here, bus 1 is the slack bus with a voltage of $0.995\angle 0°$; the nominal forecast w_0, the nominal load v_0, and the power flow solution x_0 for w_0 and v_0 are given in Table II. ■

B. Linearized Model

Now, given the power flow model in (13) and the set $\mathcal{W}$ describing the uncertainty in renewable-based generation, the objective is to obtain a set $\mathcal{X} \subseteq \mathbb{R}^{n+m-1}$ that contains all possible values that x can take. In general, given the nonlinear

TABLE II: Four-bus system nominal power flow solution.

w_0	$P^0_{g_2}$ 0.4	$Q^0_{g_2}$ 0	$P^0_{g_3}$ 0.3	$Q^0_{g_3}$ 0	$P^0_{g_4}$ 0.5	$Q^0_{g_4}$ 0
v_0	$P^0_{l_2}$ 0.8	$Q^0_{l_2}$ 0.25	$P^0_{l_3}$ 0.5	$Q^0_{l_3}$ 0.1	$P^0_{l_4}$ 0.9	$Q^0_{l_4}$ 0.5
x_0	V^0_2 0.987	θ^0_2 $-0.124°$	V^0_3 0.972	θ^0_3 $-0.273°$	V^0_4 0.965	θ^0_4 $-0.302°$

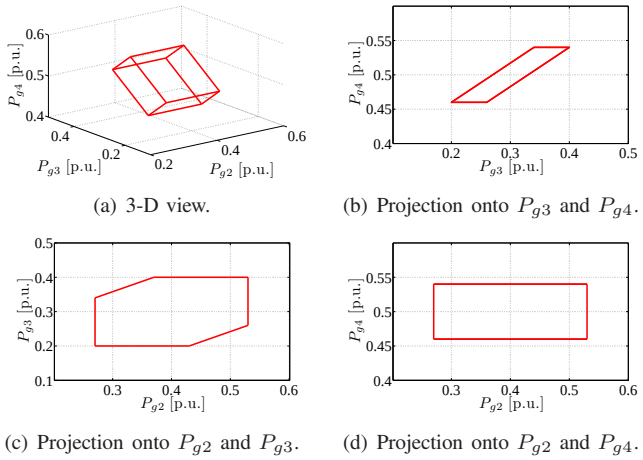

(a) 3-D view.

(b) Projection onto P_{g3} and P_{g4}.

(c) Projection onto P_{g2} and P_{g3}.

(d) Projection onto P_{g2} and P_{g4}.

Fig. 7: Four-bus system input uncertainty set.

nature of the mapping $f(\cdot)$, it is not a trivial task to obtain $\mathcal{X}$; thus we resort to approximating $\mathcal{X}$ by a set that results from applying the model obtained from linearizing (13).

Let $x = x_0 + \Delta x$, where x_0 denotes the solution to (13) with $w = w_0$, $u = u_0$, and $v = v_0$, and Δx results from $\Delta w := w - w_0$ with $w \in \mathcal{W}$. Let $\Delta u := u - u_0$ denote the change in active power arising from conventional sources at PV buses in response to Δw. Then, for Δw sufficiently small, we have

$$\Delta u + \Delta w \approx J \Delta x, \tag{14}$$

where $J = \frac{\partial f}{\partial x}\Big|_{x_0}$, with $f(\cdot)$ as defined in (13), denotes the power flow Jacobian. Now, we specify how Δu changes with Δw. The simplest choice is to assume that Δu does not change with Δw, the interpretation for which is that the slack bus is responsible for balancing the system. Another option that reflects more accurately the power balancing process in the network, which is along the lines used by the authors in [23] to formulate the so-called *governor power flow*, is to assume that the power generated by the i^{th} conventional power source changes with Δw proportionally to the total active power imbalance introduced by Δw. Thus, let Δu_i denote the i^{th} entry of Δu, and Δw_j denote the j^{th} entry of Δw; then,

$$\Delta u_i = \frac{\gamma_i}{\sum_{l \in \mathcal{A}} \gamma_l} \sum_j \Delta w_j, \tag{15}$$

where $\mathcal{A}$ contains the indices of all the power sources (including the slack bus), and the γ_l's are some positive constants that define how each power source responds (in terms of providing active power) to the net change in renewable-based generation. Note that in (15), although, we only consider the PV buses, by including the slack bus in the definition of $\mathcal{A}$, we also ensure that, beyond providing for losses, the slack bus also participates in power mismatch balancing. Now, we write (15) compactly as

$$\Delta u = B \Delta w, \tag{16}$$

where $B = [b_{ij}]$, with $b_{ij} = \frac{\gamma_i}{\sum_{l \in \mathcal{A}} \gamma_l}$, $\forall j$, which we can

combine with (13) to obtain

$$(I+B)\Delta w \approx J\Delta x. \tag{17}$$

As stated before, J is the power flow Jacobian evaluated at $x = x_0$, which is guaranteed to exist and be invertible if the power flow converges to that solution. Thus, near the nominal solution x_0,

$$\Delta x \approx M\Delta w, \tag{18}$$

where $M = J^{-1}(I+B)$. It is important to note that in radial systems with a single power source, $B = 0$; thus $M = J^{-1}$.

Since we assume that $\mathcal{W}$ is a parallelotope centered around $w = w_0$, it follows that $\Delta w \in \Delta\mathcal{W}$, where $\Delta\mathcal{W}$ is a parallelotope with the same shape and orientation as $\mathcal{W}$ but centered around $w = 0$, i.e., in geometric terms, $\Delta\mathcal{W}$ results from a translation of all the points in $\mathcal{W}$ a distance $\|w_0\|_2$ in the direction of $-w_0$. Then, the linearized model in (18) has the same form as (2); thus in line with the ideas presented in Section II, we bound $\Delta\mathcal{W}$ as follows:

$$\Delta\mathcal{W} \subseteq \bigcap_i \Delta\mathcal{E}_i, \tag{19}$$

with $\Delta\mathcal{E}_i = \{\Delta w : \Delta w^T \Delta\Psi_i^{-1} \Delta w \leq 1\}$, where $\Delta\Psi_i$ is a positive definite matrix. Then, it follows from (7) that

$$\Delta x \in \Delta\mathcal{X} \subseteq \bigcap_i \Delta\mathcal{F}_i. \tag{20}$$

with $\Delta\mathcal{F}_i = \{\Delta x : \Delta x^T \Delta\Gamma_i^{-1} \Delta x \leq 1\}$, where $\Delta\Gamma_i = M\Delta\Psi_i M^T$. Finally, we can approximate $\mathcal{X}$, i.e., the set that contains all possible values that x can take as

$$\mathcal{X} \approx \{x_0\} \oplus \Delta\mathcal{X}, \tag{21}$$

where $\oplus$ denotes the vector sum of the sets $\{x_0\}$ and $\Delta\mathcal{X}$.

Since $\Pr\{w \in \mathcal{W}\} = \alpha$, i.e., $\mathcal{W}$ captures the values that w takes with confidence level α, then $\Pr\{x \in \mathcal{X}\} \approx \Pr\{x \in \{x_0\} \oplus \Delta\mathcal{X}\} = \Pr\{w \in \{w_0\} \oplus \Delta\mathcal{W}\} = \Pr\{w \in \mathcal{W}\} = \alpha$, i.e., $\mathcal{X}$, which can be accurately approximated by $\{x_0\} \oplus \Delta\mathcal{X}$, contains the possible values that x can take with a confidence level that is approximately equal to α. In all numerical examples that follow we do not specify α as the focus is to show how to obtain the approximation of $\mathcal{X}$ once $\mathcal{W}$ is specified and to analyze the accuracy of this approximation.

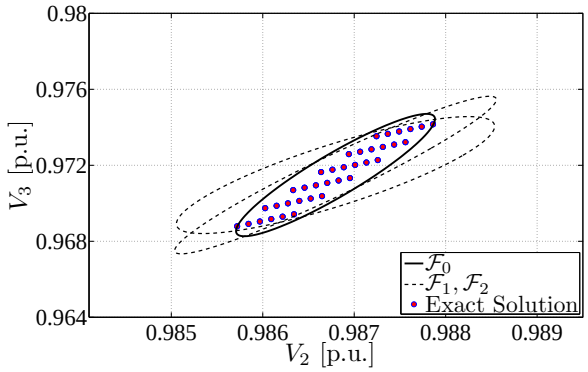

Fig. 8: Four-bus test system: nonlinear power flow solutions and state-bounding ellipsoids.

Example 4 (Four-bus system): Consider the four-bus system of Example 3. Following the ideas in Section II-B, we bound the set $\Delta\mathcal{W}$ that results from the $\mathcal{W}$ displayed in Fig. 7 with i) a minimum-trace ellipsoid $\Delta\mathcal{E}_0$, and ii) two ellipsoids $\Delta\mathcal{E}_1$ and $\Delta\mathcal{E}_2$ that are tight to $\Delta\mathcal{W}$ in the directions defined by $\eta_1 = [0.2853 \;\; -0.4755 \;\; 0.8322]^T$, and $\eta_2 = [0 \;\; 0.4961 \;\; -0.8682]^T$. We then compute the corresponding ellipsoids $\mathcal{F}_0 = \{x_0\} \oplus \Delta\mathcal{F}_0$, $\mathcal{F}_1 = \{x_0\} \oplus \Delta\mathcal{F}_1$, and $\mathcal{F}_2 = \{x_0\} \oplus \Delta\mathcal{F}_2$, that bound all possible values that Δx can take, and depict them in Fig. 8. For comparison, we also solve the exact nonlinear power flow equations for different w's sampled from $\mathcal{W}$; the corresponding solutions are depicted as points in Fig. 8. Note that the intersection of the ellipsoids obtained from the linearized power flow equations accurately bound the collection of nonlinear power flow solution points. In this case, the minimum-trace ellipsoid $\mathcal{F}_0$ provides a reasonably accurate approximation for $\mathcal{X}$. ■

C. Performance Requirements Verification

In a power system, static performance requirements include constraints in the form of interval ranges on i) the values that system states can take, and/or ii) the values that functions of these states can take. For example, bus voltage magnitudes are generally required to remain within $\pm 5\%$ of its nominal value. Also, transmission line flows, which can be obtained as a function of the states, are constrained by maximum capacity limits. Thus, once $\mathcal{X} \approx \{x_0\} \oplus \Delta\mathcal{X}$ is obtained, we can verify (with a confidence level α) whether a system meets all its performance criteria for the renewable-based generation scenario described by $\mathcal{W}$.

Let $z = h(x)$ define some performance metric of interest, where $h : \mathbb{R}^{n+m-1} \mapsto \mathbb{R}^p$, and let Φ denote a set in $\mathbb{R}^p$ defined by performance requirements. Then, for the system to meet all its performance criteria, the set $\mathcal{Z}$ that results from $\mathcal{X}$ and the mapping $h(\cdot)$, i.e., $\mathcal{Z} = \{z : z = h(x), \; x \in \mathcal{X}\}$, must be contained in Φ. As already mentioned, unless $h(\cdot)$ is linear, mapping a set through a nonlinear function is not an easy task. Therefore, as before, we resort to linearization to obtain $\mathcal{Z} \approx \{z_0\} \oplus \Delta\mathcal{Z}$, where $z_0 = h(x_0)$, and then check whether or not $\{z_0\} \oplus \Delta\mathcal{Z} \subseteq \Phi$.

1) Requirements on the values that system states can take: In this case $z = x$; thus, performance requirements constrain the values that the state x can take to some region of the state space Φ defined by the symmetric polytope

$$\Phi = \{x : |\pi_i^T (x - x_0)| \leq 1 \quad \forall i = 1, \ldots, n+m-1\}, \tag{22}$$

where $\pi_i \in \mathbb{R}^n$ is a unitary vector parallel to the i^{th} axis. Since $z = x$, then $\mathcal{Z} = \mathcal{X}$; thus in order to verify that the system meets performance requirements for any $w \in \mathcal{W}$, we need to verify whether or not $\{x_0\} + \Delta\mathcal{X} \subseteq \Phi$.

There may be situations in which performance requirements are only imposed on $q \leq n+m-1$ state variables. In order to capture this situation, we can define $z = Nx$, where N is a $q \times (n+m-1)$ matrix whose entries are zero or one depending on the entries of x that correspond to state variables over which performance requirements are imposed. In particular, for each $i = 1, \ldots, q$, there is some l_i (corresponding to the variable

x_{l_i}), satisfying $1 \leq l_i \leq n+m-1$, $l_i \neq l_j, i \neq j$, and such that $N(i,j) = 0,\ j \neq l_i$, and $N(i,l_i) = 1$. For this case, $\mathcal{Z} \approx \{z_0\} \oplus \Delta\mathcal{Z}$, with $\Delta\mathcal{Z} = \{\Delta z : \Delta z = N\Delta x,\ \Delta x \in \Delta\mathcal{X}\}$. Then, from (20), it follows that

$$\Delta z \in \Delta\mathcal{Z} \subseteq \bigcap_i \Delta\mathcal{G}_i. \tag{23}$$

with $\Delta\mathcal{G}_i = \{\Delta z : \Delta z^T (N\Delta\Gamma_i N^T)^{-1} \Delta z \leq 1\}$. By defining N to be a $2\times(n+m-1)$ or a $3\times(n+m-1)$, the resulting $\mathcal{G}_i$'s are 2- or 3-dimensional ellipsoids—an important consideration when visualizing the results of higher-order systems.

2) Requirements on the values that functions of the states can take: The procedure described above can be extended to the general case where $z = h(x)$, for some $h : \mathbb{R}^{n+m-1} \mapsto \mathbb{R}^p$ defining some performance metrics of interest, e.g., active power flow through transmission lines. In this case,

$$\Phi = \{z : |\pi_i^T (z - z_0)| \leq 1 \quad \forall i = 1, \ldots, p\}. \tag{24}$$

where $z_0 = h(x_0)$, and $\pi_i \in \mathbb{R}^s$ with all its entries equal to zero except for the i^{th}, which is equal to one. Now, for $\Delta x = x - x_0$ and $\Delta z = z - z_0$, we have

$$\Delta z \approx L\Delta x, \tag{25}$$

where $L = \frac{\partial h}{\partial x}\big|_{x_0}$. In the particular case when $h(\cdot)$ relates the system states and line power flows, the entries of the matrix $T = LM$ are in fact the generation shift factors (see, e.g., [24]). Finally, in this case, we have $\mathcal{Z} \approx \{z_0\} \oplus \Delta\mathcal{Z}$, with $\Delta\mathcal{Z} = \{\Delta z : \Delta z = L\Delta x,\ \Delta x \in \Delta\mathcal{X}\}$, and the same procedure described in (23), replacing N by L, can be used to obtain a tight upper bound on $\Delta\mathcal{Z}$.

Example 5 (Four-bus system): Consider the four-bus system of Examples 3 and 4. We assess whether or not the excursions in states V_2 and V_3 violate static performance requirements. By visual inspection of Fig. 8, note that $\mathcal{F}_0$ is entirely contained within the space defined by voltage requirements and hence we can conclude that the system does not violate any voltage constraints. Also as expected, the set $\mathcal{X}$ to which all $x_0 + \Delta x$ belong is more tightly bounded by the intersection of the ellipsoids $\mathcal{F}_0$, $\mathcal{F}_1$, and $\mathcal{F}_2$ than by $\mathcal{F}_0$ alone, as shown in the figure.

Next, we assess whether or not the active power flow through lines 1 (from bus 1 to 2) and 2 (from bus 2 to 3) violate corresponding requirements. The matrix $T = [t_{ij}]$ of generation shift factors is

$$T = \begin{bmatrix} -1.0070 & -1.0212 & -1.0265 \\ -0.0005 & -1.0123 & -1.0175 \\ -0.0002 & -0.0007 & -1.0032 \end{bmatrix},$$

where each entry t_{ij} represents the sensitivity of the i^{th} line flow with respect to the active power injection at the j^{th} bus. In Fig. 9, we plot the line flow bounding ellipsoid $\mathcal{F}_0$, corresponding to the minimum-trace input-bounding ellipsoid $\mathcal{E}_0$, along with $\mathcal{F}_1$ and $\mathcal{F}_2$, corresponding to $\mathcal{E}_1$ and $\mathcal{E}_2$, respectively. We also plot the exact line flow solution points obtained from the nonlinear power flow equations by sampling the input space; note that all these points are contained in $\mathcal{F}_0$ and $\mathcal{F}_1 \cap \mathcal{F}_2$. ■

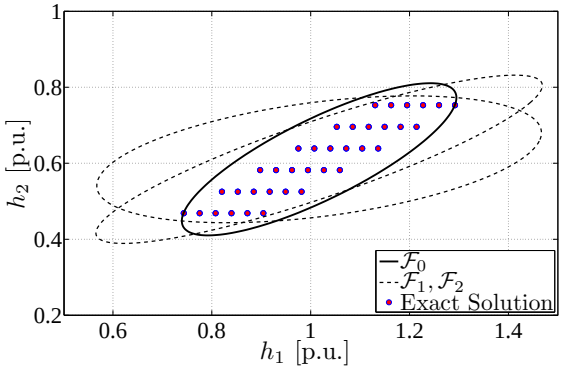

Fig. 9: Four-bus test system: nonlinear line flow solutions and corresponding bounding ellipsoids.

D. Asymmetric Input Uncertainty Set

The input uncertainty model considered so far assumes that w takes on values in a parallelotope $\mathcal{W}$ centered around some nominal value w_0, i.e., there is an underlying symmetry assumption in the bounds around w_0 that constrain the possible values of power injections of each renewable-based generator. In this section, we discuss how to extend the ideas presented so far to the case where the bounds constraining w are not symmetrically centered around w_0. We generalize the definition of the input set $\mathcal{W}$ in (3) to be

$$\mathcal{W} = \{w : w = w_0 + \sum_{j=1}^{s} \alpha_j g_j,\ \beta_j - 1 \leq \alpha_j \leq \beta_j + 1\}, \tag{26}$$

where each β_j takes on some value in the interval $[-1, 1]$. Whenever $\beta_j \neq 0$ for some j, the resulting set is no longer centered around the nominal value w_0, i.e., some of the hyperfaces of $\mathcal{W}$ defining the bounds on w are no longer equidistant from the center w_0. As defined in (26), the set $\mathcal{W}$ can capture, scenarios with asymmetries in the forecast error.

As before, given (13) and the set $\mathcal{W}$ in (26), the objective is to obtain a set $\mathcal{X}$ that contains all possible values that x can take. In order to do so, the ideas discussed in Section III-B can be tailored to the new setting where $\mathcal{W}$ is no longer centered around w_0. The first step is to redefine the input set as follows:

$$\mathcal{W} = \{w : w = w_0^* + \sum_{j=1}^{s} \gamma_j g_j,\ -1 \leq \gamma_j \leq +1\}, \tag{27}$$

where $w_0^* = w_0 + \sum_{j=1}^{s} \beta_j g_j$, i.e., $\mathcal{W}$ is a parallelotope symmetrically centered around $w_0^* = w_0 + \sum_{j=1}^{s} \beta_j g_j$. The rest of the procedure is similar to the one described in (14)–(21), with w_0^* and x_0^* replacing w_0 and x_0, respectively, resulting in

$$\mathcal{X} \approx \{x_0^*\} \oplus \Delta\mathcal{X} \subseteq \{x_0^*\} \oplus \bigcap_i \Delta\mathcal{F}_i, \tag{28}$$

where $\Delta\mathcal{F}_i$ is as defined in (20) and $\Delta\mathcal{X} = \{\Delta x : \Delta x = M \sum_{j=1}^{s} \gamma_i g_i\}$

Example 6 (Four-bus system): Consider the four-bus system introduced in Example 3, with asymmetrical input bounds of $\beta_1 = 0.286$, $\beta_2 = -0.5$, and $\beta_3 = 0.167$ corresponding to $g_1 = [0.07\ 0\ 0]^T$, $g_2 = [0\ 0.06\ 0]^T$, and $g_3 = [0\ 0\ 0.12]^T$,

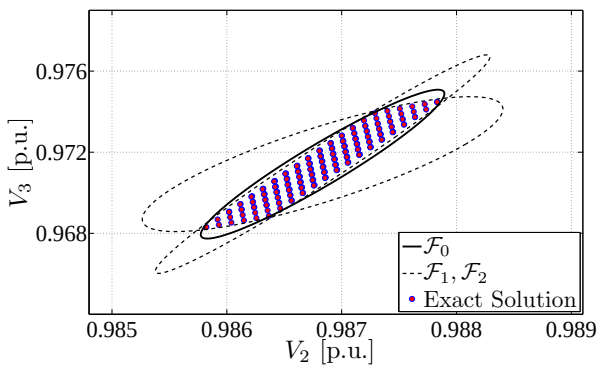

Fig. 10: Four-bus system: nonlinear line flow solutions and bounding ellipsoids for asymmetrical power injection forecast.

respectively. Applying the procedure just described, we obtain w_0^* to be $[0.42\ 0.27\ 0.52]^T$. We bound the input set $\mathcal{W}$ with a minimum-volume ellipsoid $\mathcal{E}_0$, and two ellipsoids $\mathcal{E}_1$ and $\mathcal{E}_2$ that are tight along the directions defined by $\eta_1 = \frac{g_1}{\|g_1\|}$ and $\eta_2 = \frac{g_2}{\|g_2\|}$. In Fig. 10, we plot the resulting bounding ellipsoids $\mathcal{F}_0$, $\mathcal{F}_1$, and $\mathcal{F}_2$, along with nonlinear power flow solutions obtained by sampling the input space. ■

E. Very Large Variations in Renewable-Based Power

Up to this point, we have only considered cases with sufficiently small uncertainty variations in renewable-based power injections around some nominal forecast w_0, for which the use of (14)—a linearization of the power flow equations around a *single* x_0 resulting from w_0—is justified. This approach can be justified when the variations in renewable-based power injections are interpreted as the forecast error (with some confidence level α) around the nominal forecast w_0. In some cases, however, we may be interested in characterizing the values that bus voltage magnitudes and angles can take for the worst-case variability scenario, i.e., when the power injected by each renewable-based resource i can vary between 0 and its maximum power output $\overline{w}_i$ (in this case, $\alpha = 1$). In this section, we extend the ideas presented thus far to the cases where the variations in w may not be sufficiently small for the single linearization around x_0 approach to be sufficiently accurate.

Consider the input uncertainty set $\mathcal{W}$ (a parallelotope) as defined in (3); this set can be described as the union of a finite collection of l disjoint subsets $\{\tilde{\mathcal{W}}_1, \tilde{\mathcal{W}}_2, \ldots, \tilde{\mathcal{W}}_l\}$, i.e., $\mathcal{W} = \bigcup_{i=1}^{l} \tilde{\mathcal{W}}_i$, where $\tilde{\mathcal{W}}_i \bigcap \tilde{\mathcal{W}}_j = \emptyset,\ \forall i \neq j$. While the shape of the $\tilde{\mathcal{W}}_i$'s could be arbitrary as long as they form a partition of $\mathcal{W}$, we choose them to be parallelotopes with the same shape and orientation as $\mathcal{W}$ and all of equal size; the idea is graphically depicted in Fig. 11 for a two-dimensional set. The centers of all the $\tilde{\mathcal{W}}_i$'s can be obtained from (3) and are given by

$$\mathcal{C} = \{w : w = w_0 + \sum_{j=1}^{s} \alpha_j g_j,\ \alpha_j = \pm(1+2k)/(2n_j), \\ k = 0, 1, ..., n_j - 1\}, \tag{29}$$

where $2n_j$ is the number of segments into which the segment that spans the set $\mathcal{W}$ in the direction of the j^{th} axis is divided.

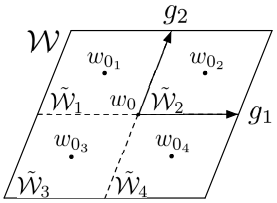

Fig. 11: Input uncertainty set partition.

Then, $\tilde{\mathcal{W}}_i$, which corresponds to $w_{0_i} \in \mathcal{C}$, is described by

$$\tilde{\mathcal{W}}_i = \{w : w = w_{0_i} + \sum_{j=1}^{s} \alpha_j g_j,\ -1/(2n_j) \leq \alpha_j \leq 1/(2n_j)\}$$

Each $\tilde{\mathcal{W}}_i$ is constructed, via appropriate choice of n_j, so that the variations in w around w_{0_i} are sufficiently small such that $\Delta w \approx J_i \Delta x$, where J_i is the power flow Jacobian evaluated at $x = x_{0_i}$, i.e., the power flow solution that corresponds to w_{0_i}. In this way, the problem is divided into several subproblems. By applying the same ideas in Section III-B to each $\tilde{\mathcal{W}}_i$, we obtain $\tilde{\mathcal{X}}_i$, the set that bounds all bus voltage magnitudes and angles corresponding to variations in $\tilde{\mathcal{W}}_i$. Finally, the set $\mathcal{X}$ that bounds all possible values that bus voltage magnitudes and angles can take as a result of $\mathcal{W}$ is given by

$$\mathcal{X} = \bigcup_{i=1}^{l} \tilde{\mathcal{X}}_i. \tag{30}$$

Example 7 (Four-bus system): Consider the four-bus system introduced in Example 3. Let the input set $\mathcal{W}$ be defined by $w_0 = [P_{g2}^0\ P_{g3}^0\ P_{g4}^0]^T = [0.4\ 0.3\ 0.5]^T$ and $g_1 = [0.4\ 0\ 0]^T$, $g_2 = [0\ 0.3\ 0]^T$, $g_3 = [0\ 0\ 0.5]^T$, i.e., renewable-based power injections vary between 0 and $\overline{w}_i = 2w_0$. Applying the ideas introduced for large input variations, we divide the uncertainty interval in each renewable generator into two equal-length segments such that $\mathcal{W} = \bigcup_{i=1}^{8} \tilde{\mathcal{W}}_i$. We then bound each $\tilde{W}_i$ with a minimum-trace ellipsoid $\tilde{\mathcal{E}}_i$. The resulting ellipsoids are projected onto the subspace defined by the P_{g2}-P_{g3} plane and shown in Fig. 12(a). We have also included the minimum-trace bounding ellipsoid for the original uncertainty set $\mathcal{W}$, $\mathcal{E}_0$, along with the input space sample points for computing the nonlinear power flow solutions. Figure 12(b) shows the corresponding state-bounding ellipsoids $\tilde{\mathcal{F}}_i$ (computed from each $\tilde{\mathcal{E}}_i$), the state-bounding ellipsoid $\mathcal{F}_0$ (computed from $\mathcal{E}_0$), and the nonlinear power flow solutions projected onto the subspace defined by the V_2-V_3 plane. From this large variability case study, we conclude that bounding set $\mathcal{X}$ can indeed be approximated to a high-fidelity by $\mathcal{X} = \bigcup_{i=1}^{8} \tilde{\mathcal{X}}_i \subseteq \bigcup_{i=1}^{8} \tilde{\mathcal{F}}_i$. In the detail of Fig. 12(b), we note that one of the $\tilde{\mathcal{F}}_i$'s captures one of the nonlinear power flow solution points that $\mathcal{F}_0$ fails to capture. Thus the union of the $\tilde{\mathcal{F}}_i$'s indeed provides a more accurate approximation than the one provided by $\mathcal{F}_0$.

We could also have utilized the ideas presented earlier to bound each $\tilde{\mathcal{W}}_i$ with multiple ellipsoids and take the intersection of the resulting state-bounding ellipsoids to obtain an even more accurate upper-bound to each of the sets $\tilde{\mathcal{X}}_i$. In this example, by considering only single bounding ellipsoids for $\mathcal{W}$ and the $\tilde{\mathcal{W}}_i$'s, we capture negative power injections, which is not realistic; however, in order to avoid cluttering the figures, we choose not to exercise these ideas. ■

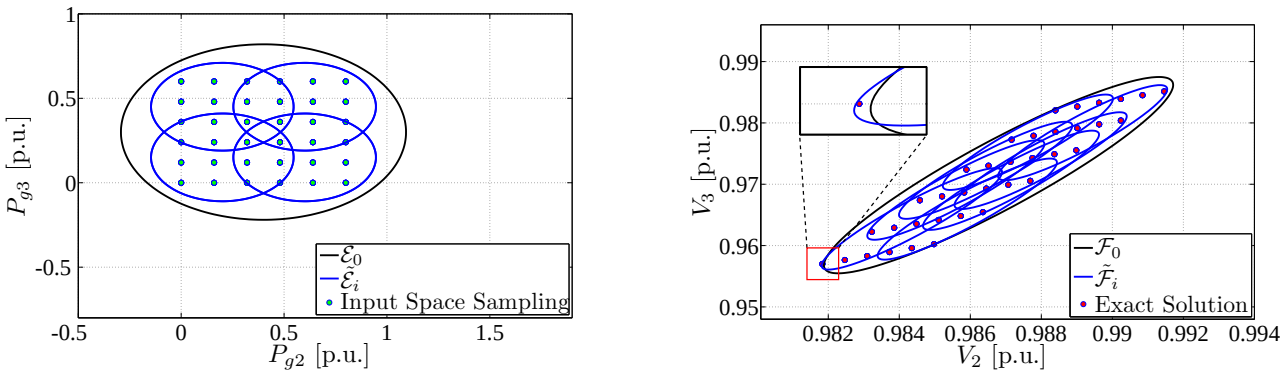

(a) Input uncertainty set and bounding ellipsoids.

(b) State-bounding ellipsoids and exact solution points.

Fig. 12: Four-bus input and state ellipsoidal bounds.

IV. Case Studies

In this section, we illustrate the concepts developed in Sections II and III by presenting the results for a 34-bus and a 123-bus system. These benchmark test systems, with a power base of 100 kVA and a voltage base of 4.16 kV, are taken from the IEEE PES Distribution System Analysis Subcommittee [25], which are modified to include power injection at a subset of buses. For each case study, we linearize the system, and using set operations, propagate uncertainty in renewable-based generation through the linearized model. Then, we examine the impact of uncertainty on bus voltage magnitudes and angles.

A. 34-bus System

The one-line diagram and complete description for this system can be found in [25]. For this system, we assume that renewable-based electricity resources are installed at buses 3, 7, 10, 15, 18, 23, 27, 29, 30, and 34, with a nominal real power injection of 1 p.u. and an uncertainty of $\pm 50\%$ (± 0.5 p.u.) around the nominal value. We bound the power injection space with a minimum-trace ellipsoid and compute the corresponding state-bounding ellipsoid. The resulting ellipsoid is projected onto the V_2-V_{34} plane and shown in Fig. 13(a). We also sample the input power injection space and obtain the corresponding solutions of the linearized power flow as well as the exact solutions of the nonlinear power flow and depict them with squares and circles, respectively. As expected, the resulting ellipsoidal bounding set $\mathcal{F}_0$ contains all the linearized power flow solutions with the extrema coinciding with the edge of the ellipsoid. The linearization is fairly accurate; only one nonlinear solution corresponding to the lower extreme point of the input sample space is not contained in the linearized solution set. For this case study, we computed the percent error between the voltage magnitudes obtained through linearized power flow and nonlinear power flow for each sample point and found the maximum to be only 3.14%. From the figure, we can also conclude that for the uncertainty levels selected, a portion of the input space maps to a region in the solution state space that violates the voltage constraints of 1.05 p.u., which are depicted with dashed lines.

Now suppose the nominal real power injection is 0.4 p.u. at the same buses and that the uncertainty of the power injections at the affected buses have correlation. Using the notation developed in (3), we present the nonzero entries of the g_i's in Table III (each g_i is a 66-dimensional vector). In this case, we bound the input power injection with a minimum-volume ellipsoid and compute the corresponding state-bounding ellipsoid. The result is shown in Fig. 13(b) along with the linearized and exact nonlinear power flow solutions. We conclude that for the the power injection and uncertainty levels chosen, no voltage magnitude violations for buses 2 and 34 are detected.

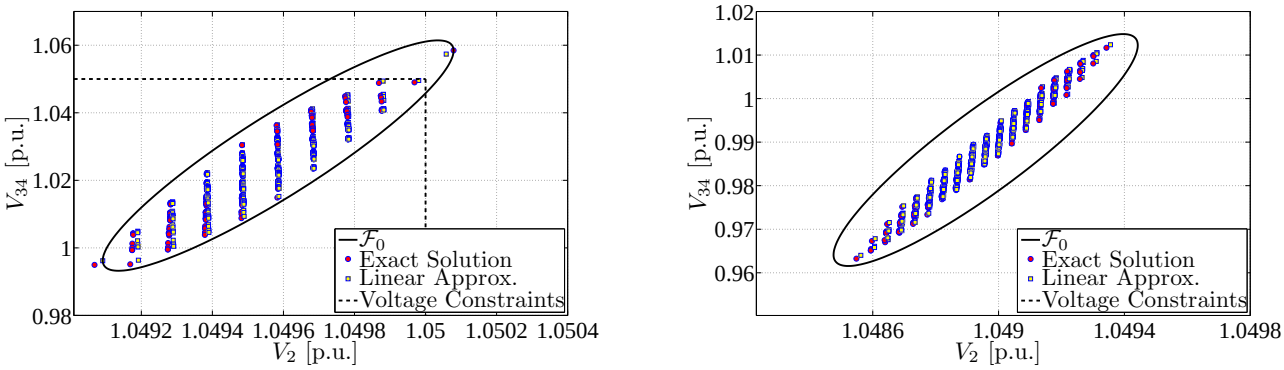

(a) Uncorrelated renewable-based power injections with variability of $\pm 50\%$ around each nominal value of 1 p.u.

(b) Correlated renewable-based power injections with variability around each nominal value of 0.4 p.u.

Fig. 13: 34-bus system: nonlinear and linearized power flow solutions, and state-bounding ellipsoid projections.

TABLE III: 34-bus System: Correlated Power Injections.

j	3	7	10	15	18	23	27	29	30	34
$g_3(j)$	0.2	0	0	0	0	0	0	0	0	0.2
$g_7(j)$	0	0.2	0	0	0	0	0	0	0	0
$g_{10}(j)$	0	0	0.2	0	0	0	0	0	0	0
$g_{15}(j)$	0	0	0	0.2	0	0	0	0	0	0
$g_{18}(j)$	0	0	0.2	0	0.2	0	0	0.2	0	0
$g_{23}(j)$	0	0.2	0	0	0	0.2	0	0	0	0
$g_{27}(j)$	0	0	0	0	0	0	0.2	0	0	0
$g_{29}(j)$	0	0	0	0.2	0	0	0	0.2	0	0
$g_{30}(j)$	0	0	0	0	0	0.2	0	0	0.2	0
$g_{34}(j)$	0.2	0	0	0	0	0	0.2	0	0	0.2

B. 123-bus System

A full description of the IEEE 123-bus test feeder can be found in [25]. In this case study, we show how the ellipsoidal method can be applied to asymmetrical uncertainties in the forecast. Table IV specifies where renewable-based electricity resources are installed along with their respective nominal power outputs and uncertainties in power injection. After applying the method proposed in Section III-D for handling asymmetrical forecast uncertainties, we bound the set of possible power injections with four ellipsoids, one of which, $\mathcal{E}_0$, is minimum-trace, and the other three, $\mathcal{E}_1$, $\mathcal{E}_2$, and $\mathcal{E}_3$, are bounding ellipsoids tight in the directions representing the real power injections at buses 96, 110, and 123, respectively.

Corresponding to each input ellipsoid $\mathcal{E}_0$, $\mathcal{E}_1$, $\mathcal{E}_2$, and $\mathcal{E}_3$, we obtain four bounding ellipsoids for the set containing the variations in x, whose projections onto the V_{103}-V_{123} plane are shown in Fig. 14(a) as $\mathcal{F}_0$, $\mathcal{F}_1$, $\mathcal{F}_2$, and $\mathcal{F}_3$, respectively. The intersection of all ellipsoids in Fig. 14(a) provides a tighter bound for the linearized power flow system states than any one ellipsoid alone and is a better approximation for the exact bounding set of the nonlinear power flow system states.

Furthermore, we plot the exact power flow solutions (depicted as circles in Fig. 14(a)) computed by sampling the extrema of the input space. As in the 34-bus case, all of the solution points lie within the intersection of the ellipsoids except for one lower extreme point, which can be attributed to the error resulting from linearization. Again, we computed the maximum error of the voltage magnitudes between the linearized power flow and nonlinear power flow to be only 1.428% for this case study. Therefore, with this particular level of uncertainty in power injection, the linearization provides an accurate estimate for the nonlinear power flow solutions.

In addition, corresponding to each input ellipsoid described above, we obtain four bounding sets containing the variations in real line flow, whose projections onto h_2 (flow on line 2 from bus 2 to 3) and h_{102} (flow on line 102 from bus 73 to 103) are shown in Fig. 14(b). Again, we display the exact line flow quantities computed by sampling the input space (depicted as points). In this case, the intersection of the line flow bounding ellipsoids in Fig. 14(b) contains all line flow variations.

In order to demonstrate the scalability of our method to systems with a large number of uncertain power injections, we have computed the state-bounding ellipsoids for cases where renewable-based electricity resources are installed at 15 buses, 30 buses, 50 buses, and 70 buses. For each of these test cases, we assume that all renewable-based nominal power injections are 1.0 p.u., with variability levels ranging between $\pm 10\%$ (± 0.1 p.u.) and $\pm 70\%$ (± 0.7 p.u.). Figure 15 shows the projections of the state-bounding ellipsoids computed from the minimum-trace input-bounding ellipsoids along with the voltage constraint bounds. In addition, for the case with renewable-based generation in 15 buses shown in Fig. 15(a), we include the nonlinear power flow solutions to show that our method does indeed provide a high-fidelity ellipsoidal approximation to the actual reach set. For the other three cases in Figs. 15(b)–15(d), we do not include the nonlinear power flow solutions due to computational power limitations

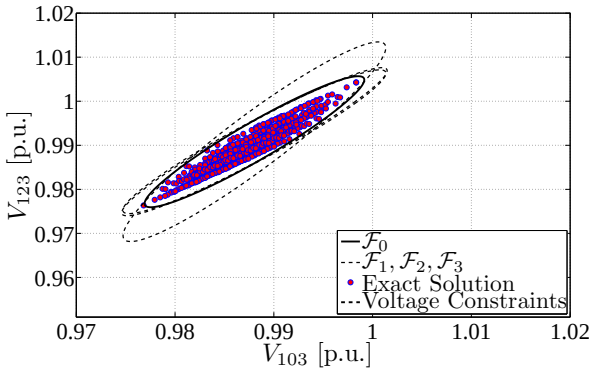

(a) Ellipsoidal bounds and exact solutions of system states.

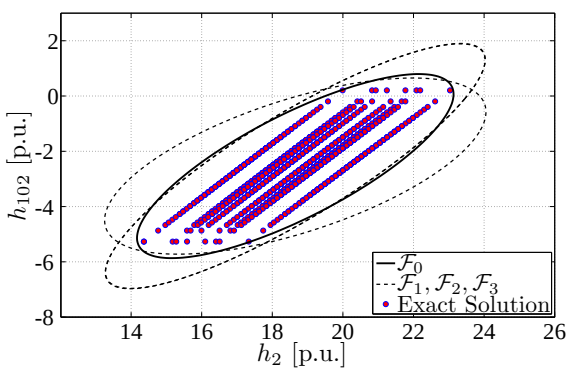

(b) Ellipsoidal bounds and exact solutions of line flows.

Fig. 14: 123-bus system: nonlinear power flow solutions and projections of state- and line-flow-bounding ellipsoids for asymmetrical power injections.

TABLE IV: 123-bus System: Data for Renewable-Based Asymmetrical Power Injections.

Bus	80	95	96	103	108	110	115	121	122	123
Nominal Value [p.u.]	1.5	1	1.5	1	1	1.5	1	1	1	1.5
Positive Variation [p.u.]	0.4	0.6	0.2	0.4	0.4	0.1	0.1	0.1	0.2	0.4
Negative Variation [p.u.]	0.8	0.2	0.7	0.7	0.6	0.5	0.3	0.7	0.5	0.5

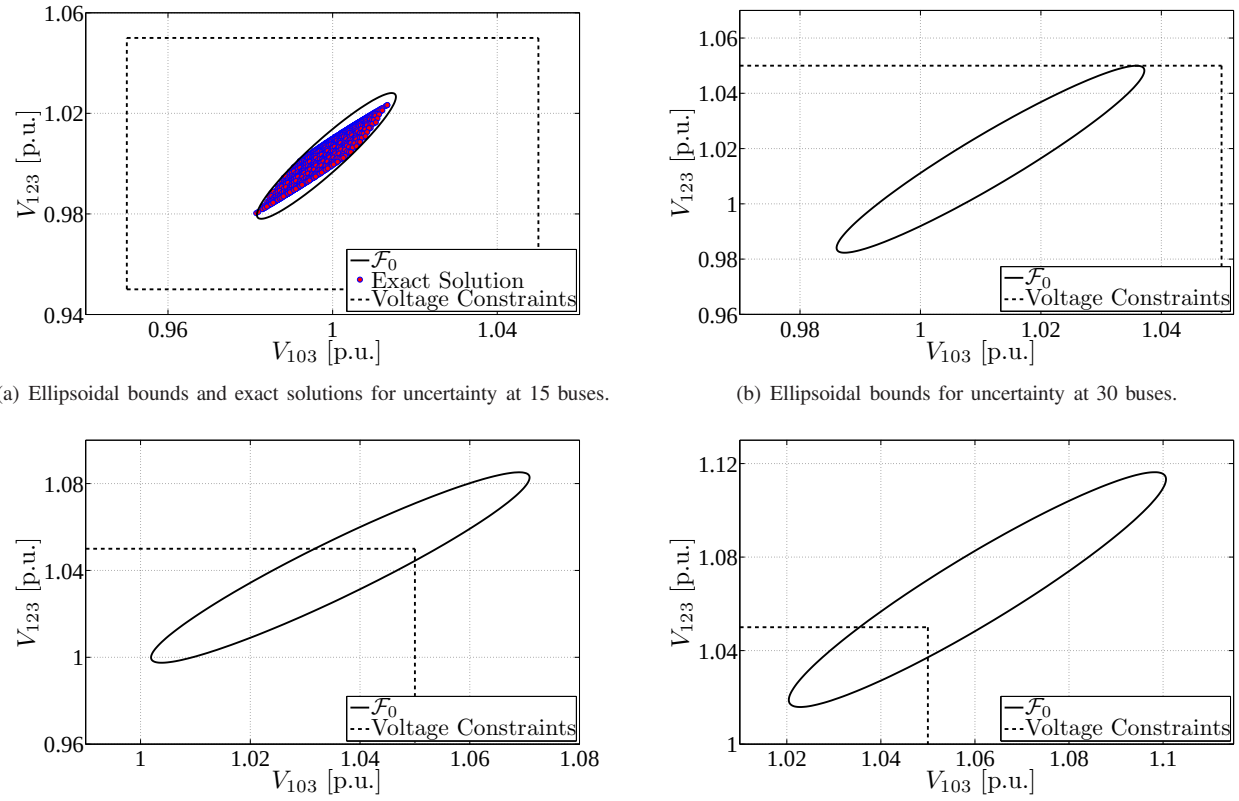

(a) Ellipsoidal bounds and exact solutions for uncertainty at 15 buses.

(b) Ellipsoidal bounds for uncertainty at 30 buses.

(c) Ellipsoidal bounds for uncertainty at 50 buses.

(d) Ellipsoidal bounds for uncertainty at 70 buses.

Fig. 15: 123-bus system: projections of state-bounding ellipsoids for different number of buses with renewable-based power.

of our computer platform (Intel Core 2 Quad 8400 processor at 2.66 GHz). Note that for the cases in Figs. 15(c)–15(d), variability in renewable-based generation may result in voltage violations.

V. Performance Evaluation

In this section, the computation time of our method is evaluated against those of solving the linearized and nonlinear power flows. For the ellipsoidal method, we provide the amount of time required to obtain the minimum-volume ellipsoid enclosing the input uncertainty space $\mathcal{W}$ and to compute the corresponding state-bounding ellipsoid approximation. The computation times presented for the nonlinear and linearized power flow solutions are for values corresponding to the vertices of $\mathcal{W}$.

The computation times required for each of the three test cases in Section IV are shown in Table V. As the number of buses increases, the time required to compute the nonlinear power flow solutions corresponding to the vertices of $\mathcal{W}$ grows much more quickly than that required for the linearized power flow and the ellipsoidal method. Furthermore, although the results are not shown, if interior points of the input space are also sampled, then significantly longer times are required for obtaining the corresponding nonlinear and linearized power flow solution points. Table VI presents a detailed timing breakdown for the ellipsoidal method, which includes the time required to obtain the ellipsoid that bounds the input uncertainty space and to compute the corresponding state-bounding ellipsoid. From the data, it is clear that most of the time spent for the ellipsoidal method involves finding the input-bounding ellipsoid through an optimization algorithm. If the input uncertainty ellipsoid is calculated *a priori*, then the time required for computing the corresponding state-bounding ellipsoid is about an order of magnitude less than that required to obtain linearized power flow solution points.

Table VII shows the average computation times required for computing the input- and state-bounding ellipsoids for the 123-bus system with renewable-based generation in 15, 30, 50, and 70 buses. While we can obtain the nonlinear power flow solutions in a timely fashion (about 3 hours) for up to 15 buses with renewable-generation, our ellipsoidal-based method does not have such scalability restrictions. This observation is evidenced by the computation times for each of the case studies; as the number of uncertainties in the system increases, the computation times for our method remain nearly constant. This observation can be attributed to the fact that as the number of buses with uncertain power injections increases, the size of the shape matrices describing the input- and state-bounding ellipsoids remains the same. Lastly, we want to point out that the times listed in Table VII are several orders of magnitude different from the computation times presented in Table VI because, for the large-scale uncertainty case studies, we have used a different computational method for obtaining the shape matrices of the minimum-trace bounding ellipsoids that takes advantage of the symmetry in the the input uncertainty space.

TABLE V: Comparison of Overall Computation Times [s] for for 4-, 34-, and 123-bus Systems.

	4-bus	34-bus	123-bus
Ellipsoid	1.297	2.960407	2.625423
Linear Approx.	0.000201	0.007308	0.043741
Nonlinear PF	0.100909	13.457959	173.809595

TABLE VI: Input and State-Bounding Ellipsoid Computation Times [s] for 4-, 34-, and 123-bus Systems.

	4-bus	34-bus	123-bus
Input Ellipsoid	1.296980	2.96	2.620066
State Ellipsoid	0.000022	0.000407	0.005357

TABLE VII: 123-bus System: Computation Times [s] for Different Number of Buses with Renewable-Based Power.

	15-bus	30-bus	50-bus	70-bus
Input Ellipsoid	0.00182	0.00199	0.00175	0.00178
State Ellipsoid	0.01707	0.01727	0.01707	0.01778
Total Time	0.0189	0.0192	0.0188	0.0195

VI. Concluding Remarks

This paper proposes a method to assess the impact of renewable resource electricity generation uncertainty on power system static performance. We model renewable generation as unknown-but-bounded power injections and formulate a set-theoretic method to obtain the worst-case deviations of static system states. This method allows us to determine whether system variables, e.g., bus voltage magnitudes and angles, or functions of these variables, e.g., power flows through transmission lines, remain within specified ranges as dictated by operational requirements.

As shown in the test cases, the set bounding the system states computed with our method matches closely to those obtained from repeatedly solving the nonlinear power flow for different power injections associated with various levels of uncertainty. We have also shown, with a 123-bus test case, that our method is scalable with the dimensionality and size of the system. It is computationally attractive since linear approximations are used and only several ellipsoids are required to establish an accurate approximation to the actual bounding set. As the number of buses increase, the nonlinear power flow takes much longer to compute than our method, which is also quite versatile in the sense that we can easily incorporate uncertainty in real and reactive power generations and demands alike.

Further work may include an analysis of the limits of the small-signal approximation to the power flow model. In this regard, we may wish to bound the higher-order Taylor series terms to obtain more accurate bounds for the variations in systems states caused by even deeper penetration levels than those considered in the case studies of this paper. An error analysis on the linear approximation can be conducted by bounding the higher-order terms of a Taylor series expansion with the Lagrange remainder. By including the higher-order terms, we might be able to capture solution points that may lie outside of the set obtained from the linearized model.

References

[1] B. Borkowska, "Probabilistic load flow," *IEEE Transactions on Power Apparatus and Systems*, vol. 93, no. 3, pp. 752–759, Aug. 1974.

[2] P. Jorgensen, J. Christensen, and J. Tande, "Probabilistic load flow calculation using monte carlo techniques for distribution network with wind turbines," in *Proc. of the 8th International Conference on Harmonics And Quality of Power*, vol. 2, oct 1998, pp. 1146 – 1151.

[3] C.-L. Su, "Probabilistic load-flow computation using point estimate method," *IEEE Transactions on Power Systems*, vol. 20, no. 4, pp. 1843 – 1851, Nov. 2005.

[4] A. Leite da Silva and V. Arienti, "Impact of power generation uncertainty on power system static performance," in *IEE Proc. of Generation, Transmission and Distribution C*, vol. 137, no. 4, Jul. 1990, pp. 276–282.

[5] A. Meliopoulos, G. Cokkinides, and X. Chao, "A new probabilistic power flow analysis method," *IEEE Transactions on Power Systems*, vol. 5, no. 1, pp. 182 – 190, Feb. 1990.

[6] P. Sauer, "A generalized stochastic power flow algorithm," in *Proc. of IEEE Power Engineering Society Summer Meeting*, 1978, pp. 544–9.

[7] R. Allan and A. Leite da Silva, "Evaluation methods and accuracy in probabilistic load flow solutions," *IEEE Transactions on Power Systems*, vol. PAS-100, no. 5, pp. 2539 – 2546, May 1981.

[8] P. Sauer and B. Hoveida, "Constrained stochastic power flow analysis," *Electric Power Systems Research*, vol. 5, no. 2, pp. 87 – 95, 1982.

[9] G. Anders, "Modelling operator action to balance system in probabilistic load-flow computations," *International Journal of Electric Power and Energy Systems*, vol. 4, no. 3, pp. 162 – 168, 1982.

[10] M. Brucoli, F. Torelli, and R. Napoli, "Quadratic probabilistic load flow with linearly modelled dispatch," *International Journal of Electric Power and Energy Systems*, vol. 7, pp. 138 – 146, 1985.

[11] A. Sarić and A. Stanković, "Model uncertainty in security assessment of power systems," *IEEE Transactions on Power Systems*, vol. 20, no. 3, pp. 1398–1407, Aug. 2005.

[12] L. Jaulin, M. Kieffer, O. Didrit, and E. Walter, *Applied Interval Analysis*. Springer, 2001.

[13] Z. Wang and F. Alvarado, "Interval arithmetic in power flow analysis," *IEEE Transactions on Power Systems*, vol. 7, no. 3, pp. 1341–1349, Aug. 1992.

[14] H. Mori and A. Yuihara, "Contingency screening using interval analysis in power systems," in *Proc. of the IEEE International Symposium on Circuits and Systems*, vol. 3, May 1998, pp. 444 – 447.

[15] A. Sarić and A. Stanković, "An application of interval analysis and optimization to electric energy markets," *IEEE Transactions on Power Systems*, vol. 21, no. 2, pp. 515 – 523, May 2006.

[16] Bonneville Power Administration. (2011, Oct.) BPA aggregated wind generation forecast. [Online]. Available: http://transmission.bpa.gov/Business/Operations/Wind/forecast/

[17] Y. Chen, X. Jiang, and A. Domínguez-García, "Impact of power generation uncertainty on power system static performance," in *Proc. of the North American Power Symposium*, Aug. 2011.

[18] H. Coxeter, *Regular Polytopes*. New York, NY: Dover Publications Inc., 1973.

[19] F. Schweppe, *Uncertain Dynamic Systems*. Englewood Cliffs, NJ: Prentice-Hall Inc., 1973.

[20] F. Chernousko and A. Ovseevich, "Properties of the optimal ellipsoids approximating the reachable sets of uncertain systems," *Optimization Theory and Applications*, vol. 120, no. 2, pp. 223–246, February 2004.

[21] W. H. Kersting, *Distribution System Modeling and Analysis*. New York, NY: CRC Press, 2001.

[22] Y. Makarov, P. Etingov, J. Ma, Z. Huang, and K. Subbarao, "Incorporating uncertainty of wind power generation forecast into power system operation, dispatch, and unit commitment procedures," *IEEE Transactions on Sustainable Energy*, vol. 2, no. 4, pp. 433–442, Oct. 2011.

[23] M. Lotfalian, R. Schlueter, D. Idizior, P. Rusche, S. Tedeschi, L. Shu, and A. Yazdankhah, "Inertial, governor, and AGC/economic dispatch load flow simulations of loss of generation contingencies," *IEEE Transactions on Power Apparatus and Systems*, vol. PAS-104, no. 11, pp. 3020 –3028, nov. 1985.

[24] A. J. Wood and B. F. Wollenberg, *Power Generation, Operation, and Control*. New York, NY: John Wiley & Sons, 1996.

[25] W. Kersting, "Radial distribution test feeders," *IEEE Transactions on Power Systems*, vol. 6, no. 3, pp. 975 –985, aug 1991.